

# Microneedle Patch-Mediated Treatment of Bacterial Biofilms

Junhua Xu,<sup>1</sup> Ryan Danehy,<sup>1</sup> Zheng Ao,<sup>1</sup> Hongwei Cai,<sup>1</sup> Meng Pu,<sup>2</sup> Alexandra Nusawardhana,<sup>1,3</sup> Dean Rowe-Magnus,<sup>2,3</sup> and Feng Guo<sup>1,\*</sup>

<sup>1</sup>. Department of Intelligent Systems Engineering, Indiana University, Bloomington, IN, 47405, United States

<sup>2</sup>. Department of Molecular and Cellular Biochemistry, Indiana University, Bloomington, IN, 47405, United States

<sup>3</sup>. Department of Biology, Indiana University, Bloomington, IN, 47405, United States

\*E-mail: [fengguo@iu.edu](mailto:fengguo@iu.edu)

**Abstract:** Current treatments of bacterial biofilms are limited by the poor penetration of antibiotics through their physical barrier as well as significant off-target toxicity of antibiotics and the induction of antibiotic resistance. Here we report a microneedle patch-mediated treatment for the effective elimination of biofilms by penetrating the biofilm and specifically delivering antibiotics to regions of active growth. We fabricated patches with self-dissolvable microneedles and needle tips loaded with chloramphenicol (CAM)-bearing and gelatinase-sensitive gelatine nanoparticles (CAM@GNPs). During the microneedle patch-mediated treatment, arrays of 225 microneedles simultaneously penetrates the biofilm matrix. Once inside, the microneedles dissolve and uniformly release CAM@GNPs into the surrounding area. In response to the gelatinase produced by the active bacterial community, the CAM@GNPs disassemble and release CAM into these active regions of the biofilm. Moreover, CAM@GNPs exhibited minimal off-target toxicity compared to direct CAM administration, which in turn favors wound healing. Importantly, we found that our microneedle-mediated treatment is more effective in treating *Vibrio vulnificus* biofilms than drug in free solution. We believe this new treatment strategy can be used to improve the delivery of a wide range of antimicrobial agents to biofilm-contaminated sites.

**Key words:** Biofilm; Transdermal Delivery; Microneedle Patch; Antibiotics

## 1. Introduction

Chronic wounds, such as diabetic foot ulcers, pressure ulcers, venous leg ulcers, and non-healing surgical-site infections, are a severe, worldwide problem. In the United States, around 6.5 million patients are affected by chronic wounds<sup>1-2</sup>. The annual treatment cost in 2010 was more than \$25 billion, and the burden is growing rapidly due to an aging population, increasing health care costs, and increased rates of obesity, diabetes, hypertension and cardiac arrhythmia<sup>3-5</sup>. Bacterial biofilms have been identified as a major cause of chronic wounds<sup>6-7</sup>. Biofilms are an assemblage of bacteria that attach to the surface of wounded tissues and cannot be removed by gentle rinsing. *E. coli*, *S. aureus*, and *P. aeruginosa* are the most prevalent bacterial species isolated from biofilm-contaminated wounds, and each biofilm has its own distinct phenotype<sup>8</sup>. Biofilm bacteria are enclosed in a self-synthesized matrix of hydrated extracellular polymeric substances (EPS) which are composed of polysaccharides, proteins, nucleic acids, and lipids. Biofilms exhibit increased resistance (up to a 1000-fold) to antimicrobial agents compared to planktonic bacteria cells<sup>9</sup>. The lack of antimicrobial effectiveness may be related to inefficient penetration into the biofilm, since matrix components can form a dense barrier that limits the penetration of antimicrobial agents<sup>8, 10</sup>. The net negative charge of EPS can sequester positively charged antimicrobial agents or repel negatively charged antimicrobial agents. Some bacteria can also produce enzymes such as  $\beta$ -lactamases that accumulate within biofilms and promote bacterial survival by inactivating target antibiotic molecules<sup>11</sup>.

Although many antimicrobial strategies are effective against planktonic bacteria, most antimicrobials are not capable of treating biofilms<sup>12</sup>. Current anti-biofilm approaches use bleach or other caustic agents to disinfect the wound<sup>13</sup>, which incur high health care costs and relatively low patient compliance<sup>14</sup>. Surgical debridement of infected tissues can effectively remove biofilm from the wound bed. However, biofilms are found to appear again within two days of the initial debridement<sup>15</sup> and the long-term antibiotic therapy further exacerbates the rise of antibiotic-resistant bacteria<sup>16</sup>. Thus, there is an urgent need to develop novel approaches to treat biofilms. The use of nanotechnology such as nanoparticles (e.g. metallic nanoparticles<sup>17-18</sup>, liposomes<sup>19-20</sup>, and polymer nanoparticles<sup>21</sup>) or nanosensors<sup>22-23</sup> is considered a promising antimicrobial strategy for rapid diagnosis and effective therapeutic treatment of infection<sup>24</sup>. The nanoscale drug carriers can protect antibiotics against degrading enzymes and increase contact time between the bacteria and the antibiotic<sup>25</sup>. To further enhance therapeutic agent performance, the nanoscale drug carriers have been tailored by improving targeting ability or responding to surrounding stimuli (pH, enzyme or temperature)<sup>26</sup>. Although the efficacy of antimicrobial drug delivery nanocarriers has

been extensively studied, relatively few studies exist that address the transport and penetration of nanoparticles within the biofilm itself<sup>25</sup>. Most anti-biofilm therapies target one bacterial species without considering that most infections in chronic wounds are due to the existence of polymicrobial biofilms. Thus, the ideal therapy is to apply the antibiotic agents to the biofilm, and meanwhile disrupt the biofilm's structure<sup>27</sup>.

To penetrate the compact physical barrier that biofilms present, the microneedle patch, a device engineered with microscale needle tips for transdermal drug delivery<sup>28</sup>, could be a sound approach. Unlike hypodermic needle injections, microneedle patches are generally positively viewed by the public and healthcare professions because they provide a localized, painless, low-cost, and patient-compliant administration method<sup>29-31</sup>. By engineering the material and dimension of the microneedles, and tuning the applied force to the microneedle patch, one can selectively penetrate stratum corneum<sup>32</sup> or reach capillary<sup>33</sup> with microneedle tips. This technology has been widely explored during the past decade for vaccination<sup>34-37</sup>, anti-diabetic<sup>38-40</sup>, anti-obesity<sup>41-43</sup>, anti-inflammatory<sup>44</sup>, local anaesthesia<sup>45-46</sup>, contraception<sup>47</sup>, and anti-tumor therapies<sup>48-50</sup>. For example, a cancer vaccine microneedle patch has been developed, and this patch consisted of whole tumor lysate as well as the adjuvant granulocyte-macrophage colony stimulating factor (GM-CSF). By applying this to mouse skin, the microneedle patch facilitates dendritic cells recruitment and promotes immune activation to enhance survival<sup>36</sup>. So far, microneedle patches have previously been utilized for these various therapeutic purposes, to our knowledge, but not been reported in treating local biofilm infections yet.

Herein, we report a microneedle patch-assisted antimicrobial therapy consisting of drug-loaded nanoparticles and polymeric matrix (Figure 1). The gelatine supramolecules can self-assemble and encapsulate the antibiotics chloramphenicol (CAM) to form antibiotic-encapsulated nanoparticles (CAM@GNPs), which are further integrated with a microneedle patch. Once applied to the infection site, the microneedles penetrate the EPS and physically disrupt the biofilm structure. Upon rapid dissolution of the polymer microneedles, the GNPs are exposed to gelatinase produced by resident microbial and disassociate, leading to the triggered release of the encapsulated CAM into the biofilm matrix. Compared to traditional topical use of CAM, the smart antimicrobial patch with its novel enzyme-sensing mechanism presents a promising approach for closed-loop regulation and prevention of antibiotic resistance development.

## 2. Experimental section

**Materials and cells.** All chemicals were purchased from Sigma-Aldrich. *Vibrio vulnificus* were grown overnight in Luria-Bertani (LB) growth medium at 37 °C. 10 µL of the diluted cell suspension was inoculated in each well of a 12-well plate and cultured for 1 day. PBS was added to wash off the planktonic or loosely adhered cells before the medium was changed to a fresh growth medium before the application of the microneedle patch.

**GNP and CAM@GNP preparation.** GNPs were prepared using the two-step desolation method according to our previously reported procedure<sup>51-52</sup>. Briefly, 1.25 g of gelatine (type B) was dissolved in 25ml of distilled water then 25 ml of acetone was added dropwise. The solution's supernatants were then discarded, and the gelatine was re-dissolved in 25 ml of distilled water. The pH of the solution was adjusted to 11 by adding NaOH solution (2M). Next, 75 ml of acetone was added dropwise to form the GNPs. Finally, 150 µL of 25% glutaraldehyde was added and the solution was left to stir overnight. The obtained GNPs were collected by centrifugation and washed three times with deionized water. The morphology and size of GNPs were examined on a JEM1010 transmission electron microscope at an acceleration voltage of 200 kV. The particle size distribution and zeta potential of GNPs were measured using a Zeta-sizer (Malvern Instrument, U.K.) at 25 °C.

**Drug loading and releasing tests.** To encapsulate the CAM into GNPs to form CAM@GNPs, the GNP solution was first lyophilized and then added to the CAM ethanol solution to a final concentration of 15 mg/mL with a weight ratio of 0.2, 0.5, 1.0, and 1.5, respectively. After swelling and loading of CAM into GNPs for 24 hours at room temperature, the nanoparticles were washed by centrifugation three times. Drug loading capacity and encapsulation efficiency were determined by measuring the unencapsulated CAM in the supernatant with high performance liquid chromatography (HPLC). The release profile of CAM from CAM@GNPs exposed to gelatinase was determined by introducing CAM@GNPs into HEPES buffer (50 mM HEPES, 2 mM CaCl<sub>2</sub>, pH 7.4) with gelatinase concentrations ranging from 0-1000 µg/mL in a Slide-A-Lyzer™ MINI dialysis device. The released CAM at predetermined intervals was analyzed with HPLC.

**Cytotoxicity test.** NIH 3T3 fibroblast cells were cultured as described above. The cytotoxicity of CAM, GNPs, and CAM@GNPs was assessed by the CCK-8 (cell counting kit-8) assay. Cells were seeded and pre-incubated for 24 hours in 96-well plates before the assay. Then, the medium was replaced with fresh medium containing CAM (20 µg/mL) or CAM@GNPs that have equivalent

CAM concentration. After 24 or 48 hours of incubation, 10  $\mu$ L of CCK-8 solution was added to the wells, followed by a 4-hour incubation. Finally, the absorbance values of the cells per well were determined with a microplate reader at 450 nm to analyze cell viability.

**Gelatine liquefaction.** *V. vulnificus* was inoculated by stabbing a tube containing LB growth medium with 3% w/w gelatine 4-5 times. The inoculated tubes, along with uninoculated tubes, were incubated at 37 °C. After 24 hours, the tubes were placed in a refrigerator (4 °C) for 30 minutes and tilted to observe if the medium had been hydrolyzed.

**Microneedle patch preparation.** The microneedle patch was prepared by a well-established solvent-casting method<sup>39, 53</sup>. Briefly, the GNP ethanol suspension was first deposited onto the microneedle patch. Then, the covered molds were centrifuged at 2000 g and left drying under air flow. The process was repeated three times. Afterward, PVP solution (3g of PVP dissolved in 1 mL of deionized water, with or without 1 mg/mL sulforhodamine B) was cast onto the microneedle molds. The molds were centrifuged at 2200 g for 15 min. After drying in an oven at 37 °C for 48 hours, the microneedle patches were carefully peeled off. The resulting microneedle patches were stored in a sealed 12-well plate for further study. The morphology of the microneedles was evaluated with a Leica M205FA stereomicroscope (Leica, Germany) or with a FEI Teneo scanning electron microscope (SEM). Biofilm sections were observed with an IX83 microscope (Olympus, Japan).

**Bacterial cell viability assay.** Numbers of colony forming units (CFU) were used to determine the number of viable bacteria in biofilms. The microneedle patch was applied on the biofilm for 30 seconds then the undissolved substrate was removed. The same dose of free drug solution was applied after impregnated with a 1 cm x 1 cm nitrocellulose membrane filter (Millipore, Ireland) that has same area of a microneedle patch. After 12 hours of treatment under indicated conditions, the filter paper that the biofilm was grown on was transferred to a 1.5 mL centrifuge tube and dispersed thoroughly in TSB by vortexing. Each sample was serially diluted in TSB, and 10  $\mu$ L of dilution was spot-plated onto TSB agar plates. CFU was imaged and counted after overnight incubation at 37 °C.

### 3. Results and discussion

**Nanoparticle preparation and characterization.** We chose gelatine nanoparticles (GNPs) as a drug delivery system for this study. Gelatine has been widely used in the food and pharmaceutical

industries due to its biocompatibility, low immunogenicity and biodegradability without the generation of toxic degradation products<sup>54</sup>. Gelatine is also classified as a “Generally Recognized as Safe” (GRAS) excipient by the US Food and Drug Administration (FDA). In the present work, GNPs were prepared using our previously described 2-step desolvation method<sup>51-52</sup>. To make the GNPs monodisperse, reduce aggregation and enhance stability, the low molecular weight gelatine fraction in the supernatant was discarded during the first-step desolvation. The high molecular weight gelatine fraction was then re-dissolved to form GNPs for the second desolvation step. The prepared GNPs demonstrated a discrete and uniform spherical morphology (Figure 2a) with an average diameter of  $131.6 \pm 23.7$  nm (data generated from measurement of 200 particles). The GNPs showed a narrow size distribution (PDI=0.154) with a hydrodynamic size of 197.6 nm (Figure 2b) according to dynamic light scattering (DLS) results. The surface charge of GNPs was determined by zeta potential measurements to be -12.6 mV, indicating good stability. The stability of GNPs was verified via storage at room temperature for 3 days. As shown in Figure 2b, there was no significant size change after storage, suggesting GNP stability over time.

**Drug loading and triggered release.** To efficiently encapsulate the antibiotic chloramphenicol (CAM) into GNPs, the GNP suspension was first lyophilized and then suspended in a CAM ethanol solution ( $c = 15$  mg/mL) for 24 hours with gentle agitation. Unencapsulated CAM was removed by washing with ethanol once and then washing with water three times. The nanoparticles were resuspended in water to obtain the CAM-encapsulated GNPs (CAM@GNPs). The drug encapsulation efficiency (EE) and drug loading capacity (LC) were determined by measuring unencapsulated CAM using high performance liquid chromatography (HPLC, Figure 2c). The optimal feeding ratio is 1.0(CAM weight/GNP weight) due to the EE being 41.6% and LC being 41.6%. The following experiments use this formulation.

Ideally, a drug delivery system should stay inert at physiological conditions but immediately start to release drugs in the presence of viable bacterial cells. Elevated levels of proteases, including gelatinase, have been found at active infection sites<sup>55</sup>. Therefore, we explored the possibility of utilizing the gelatinase-rich microenvironments as a trigger for drug release *in situ*. To demonstrate that the release of CAM from CAM@GNPs can be triggered by gelatinase, the release profiles of CAM@GNPs were monitored by HPLC (Figure 2d). The CAM@GNPs (3 mg/mL) were incubated in the presence of 0 to 1000  $\mu$ g/mL gelatinase in HEPES buffer (50 mM, pH 7.4) for 48 hours. As shown in Figure 2d, ~90% of the CAM was released within the first 16 hours following treatment with 1000  $\mu$ g/mL gelatinase. The release process slowed down plateaued after 24 hours

when the concentration of gelatinase was reduced to 7.5 or 300  $\mu\text{g/mL}$ . Total drug release increased with increasing gelatinase concentration (7.5  $\mu\text{g/mL}$ : 61.8%, 300  $\mu\text{g/mL}$ : 81.6%, 1000  $\mu\text{g/mL}$ : 91.9%). In contrast, only 29.4% of CAM was released from CAM@GNPs after 48 hours in the absence of gelatinase. The results were similar (34.3%) to the control group when the gelatinase was denatured via heating. These results demonstrated that CAM was released from CAM@GNPs by gelatinase in a controlled manner.

**On-target cytotoxicity.** Here, we choose *V. vulnificus* as an *in vitro* biofilm wound infection model. *V. vulnificus* is best known for causing devastating wound and septicemic infections. The fatality rate of septicemic patients is greater than 50% and *V. vulnificus* carries the highest death rate of any food-borne disease agent<sup>56</sup>. The ability of bacteria *V. vulnificus* to produce extracellular enzyme (gelatinase) was demonstrated by gelatine liquefaction tests. *V. vulnificus* was inoculated to gelatine medium and incubated for 24 hours. Afterwards, the tubes were chilled to determine the liquefaction of the gelatine. A positive gelatine liquefaction result was observed (Figure 3a). The concentration of gelatinase produced by active *V. vulnificus* ranges from 1.25 unit/mL to 4.08 unit/mL according to previous studies<sup>57</sup>. Hence, the ability to liquefy gelatine by *V. vulnificus* was demonstrated. Collectively, these results suggested that the CAM@GNPs constituted a gelatinase concentration/time-dependent delivery system for the targeted release of antibiotics within biofilms with minimal toxicity towards normal tissue.

One major limitation for the use of the antibiotics is their systemic toxicities. Numerous case reports in the IARC review have shown that CAM may induce aplastic anemia due to its cytogenetic effects in mammalian cells<sup>58</sup>. To verify that the toxicity of CAM against mammalian cells can be reduced via encapsulation into GNPs, we tested its toxicity with or without GNP encapsulation against NIH 3T3 fibroblast cells. Fibroblast cells play a vital role in wound healing where extensive cytotoxicity of CAM may affect their viability, thus hindering healing of biofilm-contaminated wounds. To test this, we incubated the cells with free CAM, empty GNPs and CAM@GNPs, respectively, for 4 hours. The concentration of CAM used in this study was 20  $\mu\text{g/mL}$  because the clinical dosage of chloramphenicol normally used against infectious diseases is 15–30  $\mu\text{g/mL}$ <sup>59</sup>. The incubation was followed by PBS washes and incubation in fresh media for 24 or 48 hours. Viable cell number was then determined using the CCK-8 assay. As shown in Figure 3b, the viable 3T3 cell number for the free CAM treated group was only 77.3% (24 hours) and 57.2% (48 hours) compared to the control group. However, the toxicity of CAM was significantly reduced after encapsulation into GNPs to form CAM@GNPs. This reduced toxicity can be attributed to the fact that 3T3 cells have relatively low gelatinase expression<sup>60</sup> and low

endocytosis of GNPs according to our previous studies<sup>52</sup>. Furthermore, since the gelatine is a well-known natural material for its excellent biocompatibility, the GNPs and CAM@GNPs groups promoted cell proliferation due to the presence of gelatine, which is in accordance with previous reports<sup>61-62</sup>. Therefore, CAM's cytotoxicity toward fibroblast cells was reduced by encapsulation in GNPs.

**Microneedle patch mediated treatment.** Biofilms produce an extracellular polymeric substance that hinders the effective delivery of therapeutics. To achieve biofilm disruption and improve antibiotics penetration while maintaining painless administration, the CAM@GNPs were further integrated into a microneedle array patch device. The microneedle patches were manufactured with water-soluble and biocompatible polyvinylpyrrolidone (PVP) via a micro-molding approach. The resulting microneedles were arranged in a 15\*15 array with 500  $\mu\text{m}$  tip-to-tip spacing. Each needle was of a pyramid shape with 200  $\mu\text{m}$  base and 600  $\mu\text{m}$  height (Figure 4 a-c). Since most of the microvasculature in the papillary dermis is 1–2 mm below the epidermal surface, each microneedle tip will penetrate into biofilms but will not have access to capillary bed<sup>33</sup>. The schematic in Figure 4b represents the nanoparticle-loaded microneedle patch fabrication process. The fluorescence images in Figure 4c represent a sulforhodamine-labeled microneedle patch with FITC-labeled GNPs, indicating GNPs were well distributed in the tip region of each tip.

Having confirmed that the microneedle patches have sharp-shaped microneedle array morphologies and that the CAM@GNPs can be successfully incorporated into the tips, we inspected whether these microneedles could effectively overcome the penetrative barrier that biofilms present. We loaded fluorescent sulforhodamine B into the microneedles to mimic the antibiotic and treated biofilms of *V. vulnificus* that expressed green fluorescent protein (GFP). The biofilm samples after microneedle patch application were bisected perpendicular to the biofilm plane. As shown in Figure 5, upon application of the microneedle patch, the integrity of the biofilm was disrupted, and the dye from the microneedle patch effectively diffused into the biofilm matrix. In contrast, the dye in free solution displayed negligible penetration and diffusion. The optical image of the microneedle patch revealed that the tips had disappeared after application (Figure 6), further verifying the complete release of the surrogate drug. This data indicates that the microneedle patch facilitates the delivery of the payload into biofilm in an efficient manner.

Finally, we investigated the therapeutic efficacy of the CAM@GNPs-loaded patch against established bacterial biofilms (Figure 7). CAM@GNPs-loaded patches and empty patches were applied topically for 30 seconds on the biofilm, which were then returned to culture in 37 °C to evaluate viability after treatment. Equivalent free CAM concentrations were applied as a control. After incubation for the indicated time, viable *V. vulnificus* from biofilms were recovered and counted. We observed a significant decrease of 55.6% (4 hours) and 63.2% (8 hours) respectively, in colony forming unit (CFU) per milliliter in the CAM@GNPs patch compared to free drug in solution. The lower efficacy of the free drug solution is consistent with previous reports suggesting insufficient penetration of the free drug following topical application to exert an antibiofilm effect<sup>63-64</sup>. The enhanced antibiofilm activity of CAM@GNPs microneedle patch is achieved through a better distribution of CAM, a more disrupted EPS matrix, and a specific enzyme-triggered drug release.

#### **4. Conclusion**

In summary, we report a microneedle patch-based drug delivery platform for local and specific drug release within biofilms. By combining the advantages of the biofilm-disrupting microneedle patch and infection microenvironment-responsive GNPs, our GNP-loaded microneedle patch exhibited a notably enhanced therapeutic outcome. Due to the flexibility and ease of preparation, this platform can be designed not only for chloramphenicol but also for other antibiofilm agents with similar penetration/toxicity issues. These microneedle patches have potential as a general surface disinfectant as well as an antiseptic to promote wound healing. Future studies will explore microneedle patch performance in combating *in vivo* biofilms. It is envisioned that this novel microneedle patch drug delivery system might serve as an enhanced treatment protocol for biofilm infections to facilitate clearance and wound healing in clinical settings.

#### **Acknowledgments**

We acknowledge Dr. Cheng Kao's kind discussion. This project was supported by the Departmental Start-Up Fund and the Vice Provost for the Research through the Faculty Research Support Program of Indiana University Bloomington.

## References

- (1) Sen, C. K.; Gordillo, G. M.; Roy, S.; Kirsner, R.; Lambert, L.; Hunt, T. K.; Gottrup, F.; Gurtner, G. C.; Longaker, M. T. Human skin wounds: A major and snowballing threat to public health and the economy. *Wound Repair Regen* **2009**, *17* (6), 763-771.
- (2) Frykberg, R. G.; Banks, J. Challenges in the Treatment of Chronic Wounds. *Adv Wound Care* **2015**, *4* (9), 560-582.
- (3) Clinton, A.; Carter, T. Chronic Wound Biofilms: Pathogenesis and Potential Therapies. *Lab Med* **2015**, *46* (4), 277-84.
- (4) Driver, V. R.; Blume, P. A. Evaluation of Wound Care and Health-Care Use Costs in Patients with Diabetic Foot Ulcers Treated with Negative Pressure Wound Therapy versus Advanced Moist Wound Therapy (vol 104, pg 147, 2014). *J Am Podiat Med Assn* **2014**, *104* (4), 374-374.
- (5) Goldberg, E.; Beitz, J. M. The lived experience of diverse elders with chronic wounds. *Ostomy Wound Manage* **2010**, *56* (11), 36-46.
- (6) Costerton, J. W.; Stewart, P. S.; Greenberg, E. P. Bacterial biofilms: a common cause of persistent infections. *Science* **1999**, *284* (5418), 1318-22.
- (7) James, G. A.; Swogger, E.; Wolcott, R.; Pulcini, E.; Secor, P.; Sestrich, J.; Costerton, J. W.; Stewart, P. S. Biofilms in chronic wounds. *Wound Repair Regen* **2008**, *16* (1), 37-44.
- (8) Stewart, P. S.; Costerton, J. W. Antibiotic resistance of bacteria in biofilms. *Lancet* **2001**, *358* (9276), 135-8.
- (9) Smith, A. W. Biofilms and antibiotic therapy: is there a role for combating bacterial resistance by the use of novel drug delivery systems? *Adv Drug Deliv Rev* **2005**, *57* (10), 1539-50.
- (10) Szomolay, B.; Klapper, I.; Dockery, J.; Stewart, P. S. Adaptive responses to antimicrobial agents in biofilms. *Environ Microbiol* **2005**, *7* (8), 1186-91.
- (11) Bagge, N.; Ciofu, O.; Skovgaard, L. T.; Hoiby, N. Rapid development in vitro and in vivo of resistance to ceftazidime in biofilm-growing *Pseudomonas aeruginosa* due to chromosomal beta-lactamase. *Apmis* **2000**, *108* (9), 589-600.
- (12) Percival, S. L.; Bowler, P.; Woods, E. J. Assessing the effect of an antimicrobial wound dressing on biofilms. *Wound Repair Regen* **2008**, *16* (1), 52-7.
- (13) Marion-Ferey, K.; Pasmore, M.; Stoodley, P.; Wilson, S.; Husson, G. P.; Costerton, J. W. Biofilm removal from silicone tubing: an assessment of the efficacy of dialysis machine decontamination procedures using an in vitro model. *J Hosp Infect* **2003**, *53* (1), 64-71.
- (14) Lynch, A. S.; Robertson, G. T. Bacterial and fungal biofilm infections. *Annu Rev Med* **2008**, *59*, 415-28.
- (15) Wolcott, R. D.; Rumbaugh, K. P.; James, G.; Schultz, G.; Phillips, P.; Yang, Q.; Watters, C.; Stewart, P. S.; Dowd, S. E. Biofilm maturity studies indicate sharp debridement opens a time-dependent therapeutic window. *J Wound Care* **2010**, *19* (8), 320-8.
- (16) Levy, S. B.; Marshall, B. Antibacterial resistance worldwide: causes, challenges and responses. *Nat Med* **2004**, *10* (12 Suppl), S122-9.

- (17) Zhao, Y.; Ye, C.; Liu, W.; Chen, R.; Jiang, X. Tuning the composition of AuPt bimetallic nanoparticles for antibacterial application. *Angew Chem Int Ed Engl* **2014**, *53* (31), 8127-31.
- (18) Zhao, Y.; Tian, Y.; Cui, Y.; Liu, W.; Ma, W.; Jiang, X. Small molecule-capped gold nanoparticles as potent antibacterial agents that target Gram-negative bacteria. *J Am Chem Soc* **2010**, *132* (35), 12349-56.
- (19) Drulis-Kawa, Z.; Dorotkiewicz-Jach, A. Liposomes as delivery systems for antibiotics. *Int J Pharm* **2010**, *387* (1-2), 187-98.
- (20) Duncan, B.; Li, X.; Landis, R. F.; Kim, S. T.; Gupta, A.; Wang, L. S.; Ramanathan, R.; Tang, R.; Boerth, J. A.; Rotello, V. M. Nanoparticle-Stabilized Capsules for the Treatment of Bacterial Biofilms. *ACS Nano* **2015**, *9* (8), 7775-82.
- (21) Li, Y.; Zhao, Z.; Zhang, J.; Kwok, R. T. K.; Xie, S.; Tang, R.; Jia, Y.; Yang, J.; Wang, L.; Lam, J. W. Y.; Zheng, W.; Jiang, X.; Tang, B. Z. A Bifunctional Aggregation-Induced Emission Luminogen for Monitoring and Killing of Multidrug-Resistant Bacteria. *Advanced Functional Materials* **2018**, *28* (42).
- (22) Liu, T.; Lu, Y.; Gau, V.; Liao, J. C.; Wong, P. K. Rapid antimicrobial susceptibility testing with electrokinetics enhanced biosensors for diagnosis of acute bacterial infections. *Ann Biomed Eng* **2014**, *42* (11), 2314-21.
- (23) Mukherjee, M.; Menon, N. V.; Liu, X.; Kang, Y.; Cao, B. Confocal Laser Scanning Microscopy-Compatible Microfluidic Membrane Flow Cell as a Nondestructive Tool for Studying Biofouling Dynamics on Forward Osmosis Membranes. *Environ Sci Tech Let* **2016**, *3* (8), 303-309.
- (24) Guo, J.; Wang, W.; Hu, J.; Xie, D.; Gerhard, E.; Nisic, M.; Shan, D.; Qian, G.; Zheng, S.; Yang, J. Synthesis and characterization of anti-bacterial and anti-fungal citrate-based mussel-inspired bioadhesives. *Biomaterials* **2016**, *85*, 204-17.
- (25) Forier, K.; Raemdonck, K.; De Smedt, S. C.; Demeester, J.; Coenye, T.; Braeckmans, K. Lipid and polymer nanoparticles for drug delivery to bacterial biofilms. *J Control Release* **2014**, *190*, 607-23.
- (26) Allen, T. M.; Cullis, P. R. Drug delivery systems: entering the mainstream. *Science* **2004**, *303* (5665), 1818-22.
- (27) Miquel, S.; Lagrèfeuille, R.; Souweine, B.; Forestier, C. Anti-biofilm Activity as a Health Issue. *Front Microbiol* **2016**, *7*, 592.
- (28) Prausnitz, M. R.; Langer, R. Transdermal drug delivery. *Nat Biotechnol* **2008**, *26* (11), 1261-8.
- (29) Indermun, S.; Luttge, R.; Choonara, Y. E.; Kumar, P.; du Toit, L. C.; Modi, G.; Pillay, V. Current advances in the fabrication of microneedles for transdermal delivery. *J Control Release* **2014**, *185*, 130-8.
- (30) Than, A.; Liu, C.; Chang, H.; Duong, P. K.; Cheung, C. M. G.; Xu, C.; Wang, X.; Chen, P. Self-implantable double-layered micro-drug-reservoirs for efficient and controlled ocular drug delivery. *Nat Commun* **2018**, *9* (1), 4433.

- (31) Kim, Y. C.; Park, J. H.; Prausnitz, M. R. Microneedles for drug and vaccine delivery. *Adv Drug Deliv Rev* **2012**, *64* (14), 1547-68.
- (32) Ripolin, A.; Quinn, J.; Larraneta, E.; Vicente-Perez, E. M.; Barry, J.; Donnelly, R. F. Successful application of large microneedle patches by human volunteers. *Int J Pharm* **2017**, *521* (1-2), 92-101.
- (33) Blicharz, T. M.; Gong, P.; Bunner, B. M.; Chu, L. L.; Leonard, K. M.; Wakefield, J. A.; Williams, R. E.; Dadgar, M.; Tagliabue, C. A.; El Khaja, R.; Marlin, S. L.; Haghgooie, R.; Davis, S. P.; Chickering, D. E.; Bernstein, H. Microneedle-based device for the one-step painless collection of capillary blood samples. *Nature Biomedical Engineering* **2018**, *2* (3), 151-157.
- (34) Sullivan, S. P.; Koutsonanos, D. G.; Del Pilar Martin, M.; Lee, J. W.; Zarnitsyn, V.; Choi, S. O.; Murthy, N.; Compans, R. W.; Skountzou, I.; Prausnitz, M. R. Dissolving polymer microneedle patches for influenza vaccination. *Nat Med* **2010**, *16* (8), 915-20.
- (35) Demuth, P. C.; Garcia-Beltran, W. F.; Ai-Ling, M. L.; Hammond, P. T.; Irvine, D. J. Composite dissolving microneedles for coordinated control of antigen and adjuvant delivery kinetics in transcutaneous vaccination. *Adv Funct Mater* **2013**, *23* (2), 161-172.
- (36) Ye, Y.; Wang, C.; Zhang, X.; Hu, Q.; Zhang, Y.; Liu, Q.; Wen, D.; Milligan, J.; Bellotti, A.; Huang, L.; Dotti, G.; Gu, Z. A melanin-mediated cancer immunotherapy patch. *Sci Immunol* **2017**, *2* (17).
- (37) Shakya, A. K.; Lee, C. H.; Gill, H. S. Cutaneous vaccination with coated microneedles prevents development of airway allergy. *J Control Release* **2017**, *265*, 75-82.
- (38) Yu, J.; Zhang, Y.; Ye, Y.; DiSanto, R.; Sun, W.; Ranson, D.; Ligler, F. S.; Buse, J. B.; Gu, Z. Microneedle-array patches loaded with hypoxia-sensitive vesicles provide fast glucose-responsive insulin delivery. *Proc Natl Acad Sci U S A* **2015**, *112* (27), 8260-5.
- (39) Yu, J.; Qian, C.; Zhang, Y.; Cui, Z.; Zhu, Y.; Shen, Q.; Ligler, F. S.; Buse, J. B.; Gu, Z. Hypoxia and H<sub>2</sub>O<sub>2</sub> Dual-Sensitive Vesicles for Enhanced Glucose-Responsive Insulin Delivery. *Nano Lett* **2017**, *17* (2), 733-739.
- (40) Ye, Y.; Yu, J.; Wang, C.; Nguyen, N. Y.; Walker, G. M.; Buse, J. B.; Gu, Z. Microneedles Integrated with Pancreatic Cells and Synthetic Glucose-Signal Amplifiers for Smart Insulin Delivery. *Adv Mater* **2016**, *28* (16), 3115-3121.
- (41) Dangol, M.; Kim, S.; Li, C. G.; Fakhraei Lahiji, S.; Jang, M.; Ma, Y.; Huh, I.; Jung, H. Anti-obesity effect of a novel caffeine-loaded dissolving microneedle patch in high-fat diet-induced obese C57BL/6J mice. *J Control Release* **2017**, *265*, 41-47.
- (42) Zhang, Y.; Liu, Q.; Yu, J.; Yu, S.; Wang, J.; Qiang, L.; Gu, Z. Locally Induced Adipose Tissue Browning by Microneedle Patch for Obesity Treatment. *ACS Nano* **2017**, *11* (9), 9223-9230.
- (43) Than, A.; Liang, K.; Xu, S.; Sun, L.; Duan, H.; Xi, F.; Xu, C.; Chen, P. Transdermal Delivery of Anti-Obesity Compounds to Subcutaneous Adipose Tissue with Polymeric Microneedle Patches. *Small Methods* **2017**, *1* (11).

- (44) Zhang, Y.; Feng, P.; Yu, J.; Yang, J.; Zhao, J.; Wang, J.; Shen, Q.; Gu, Z. ROS-Responsive Microneedle Patch for Acne Vulgaris Treatment. *Advanced Therapeutics* **2018**, *1* (3), 1800035.
- (45) Baek, S. H.; Shin, J. H.; Kim, Y. C. Drug-coated microneedles for rapid and painless local anesthesia. *Biomed Microdevices* **2017**, *19* (1), 2.
- (46) Nayak, A.; Babla, H.; Han, T.; Das, D. B. Lidocaine carboxymethylcellulose with gelatine co-polymer hydrogel delivery by combined microneedle and ultrasound. *Drug Deliv* **2016**, *23* (2), 658-69.
- (47) Li, W.; Terry, R. N.; Tang, J.; Feng, M. H. R.; Schwendeman, S. P.; Prausnitz, M. R. Rapidly separable microneedle patch for the sustained release of a contraceptive. *Nature Biomedical Engineering* **2019**, *3* (3), 220-229.
- (48) Chen, M. C.; Lin, Z. W.; Ling, M. H. Near-Infrared Light-Activatable Microneedle System for Treating Superficial Tumors by Combination of Chemotherapy and Photothermal Therapy. *ACS Nano* **2016**, *10* (1), 93-101.
- (49) Ye, Y.; Wang, J.; Hu, Q.; Hochu, G. M.; Xin, H.; Wang, C.; Gu, Z. Synergistic Transcutaneous Immunotherapy Enhances Antitumor Immune Responses through Delivery of Checkpoint Inhibitors. *ACS Nano* **2016**, *10* (9), 8956-63.
- (50) Wang, C.; Ye, Y.; Hochu, G. M.; Sadeghifar, H.; Gu, Z. Enhanced Cancer Immunotherapy by Microneedle Patch-Assisted Delivery of Anti-PD1 Antibody. *Nano Lett* **2016**, *16* (4), 2334-40.
- (51) Li, L. L.; Xu, J. H.; Qi, G. B.; Zhao, X.; Yu, F.; Wang, H. Core-shell supramolecular gelatin nanoparticles for adaptive and "on-demand" antibiotic delivery. *ACS Nano* **2014**, *8* (5), 4975-83.
- (52) Xu, J. H.; Gao, F. P.; Liu, X. F.; Zeng, Q.; Guo, S. S.; Tang, Z. Y.; Zhao, X. Z.; Wang, H. Supramolecular gelatin nanoparticles as matrix metalloproteinase responsive cancer cell imaging probes. *Chem Commun (Camb)* **2013**, *49* (40), 4462-4.
- (53) Brambilla, D.; Proulx, S. T.; Marschalkova, P.; Detmar, M.; Leroux, J. C. Microneedles for the Noninvasive Structural and Functional Assessment of Dermal Lymphatic Vessels. *Small* **2016**, *12* (8), 1053-61.
- (54) Yamamoto, M.; Ikada, Y.; Tabata, Y. Controlled release of growth factors based on biodegradation of gelatin hydrogel. *J Biomat Sci-Polym E* **2001**, *12* (1), 77-88.
- (55) Yager, D. R.; Nwomeh, B. C. The proteolytic environment of chronic wounds. *Wound Repair Regen* **1999**, *7* (6), 433-41.
- (56) Oliver, J. D. Wound infections caused by *Vibrio vulnificus* and other marine bacteria. *Epidemiol Infect* **2005**, *133* (3), 383-91.
- (57) Smith, G. C.; Merkel, J. R. Collagenolytic activity of *Vibrio vulnificus*: potential contribution to its invasiveness. *Infect Immun* **1982**, *35* (3), 1155-6.
- (58) Giuliani, F.; Koller, T.; Wurgler, F. E.; Widmer, R. M. Detection of genotoxic activity in native hospital waste water by the umuC test. *Mutat Res* **1996**, *368* (1), 49-57.
- (59) Balbi, H. J. Chloramphenicol: a review. *Pediatr Rev* **2004**, *25* (8), 284-8.

- (60) Ailenberg, M.; Silverman, M. Cytochalasin D disruption of actin filaments in 3T3 cells produces an anti-apoptotic response by activating gelatinase A extracellularly and initiating intracellular survival signals. *Biochim Biophys Acta* **2003**, *1593* (2-3), 249-58.
- (61) Dreesmann, L.; Ahlers, M.; Schlosshauer, B. The pro-angiogenic characteristics of a cross-linked gelatin matrix. *Biomaterials* **2007**, *28* (36), 5536-43.
- (62) Nichol, J. W.; Koshy, S. T.; Bae, H.; Hwang, C. M.; Yamanlar, S.; Khademhosseini, A. Cell-laden microengineered gelatin methacrylate hydrogels. *Biomaterials* **2010**, *31* (21), 5536-44.
- (63) Koo, H.; Schobel, B.; Scott-Anne, K.; Watson, G.; Bowen, W. H.; Cury, J. A.; Rosalen, P. L.; Park, Y. K. Apigenin and tt-farnesol with fluoride effects on *S. mutans* biofilms and dental caries. *J Dent Res* **2005**, *84* (11), 1016-20.
- (64) Koo, H.; Hayacibara, M. F.; Schobel, B. D.; Cury, J. A.; Rosalen, P. L.; Park, Y. K.; Vacca-Smith, A. M.; Bowen, W. H. Inhibition of *Streptococcus mutans* biofilm accumulation and polysaccharide production by apigenin and tt-farnesol. *J Antimicrob Chemother* **2003**, *52* (5), 782-9.

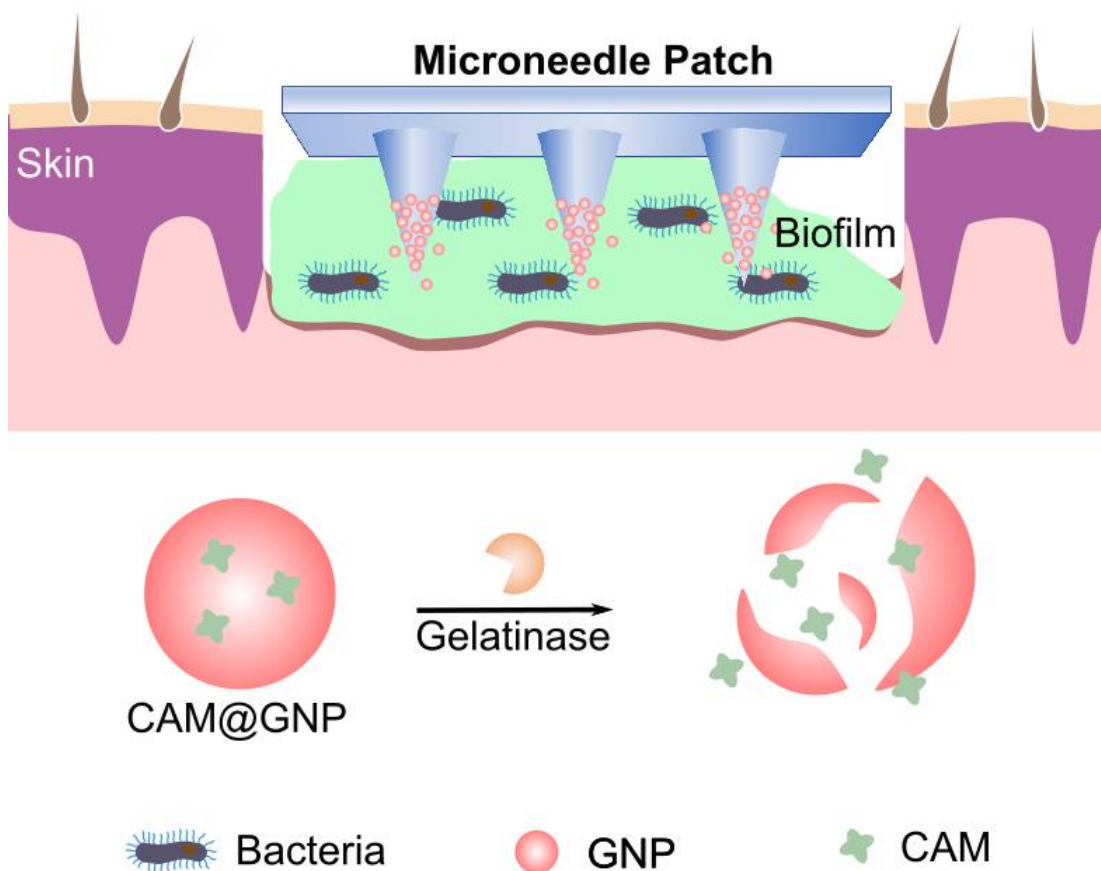


**Figure 1.** Schematic of the microneedle mediated biofilm treatment. The microneedles penetrate through and dissolve into the biofilm to transdermally release gelatine nanoparticles (GNPs) loaded with antibiotics (chloramphenicol, CAM). In response to gelatinase produced by active bacteria, the GNPs specifically release antibiotics to eliminate the pathogenic bacteria within the biofilm without off-target toxicity.

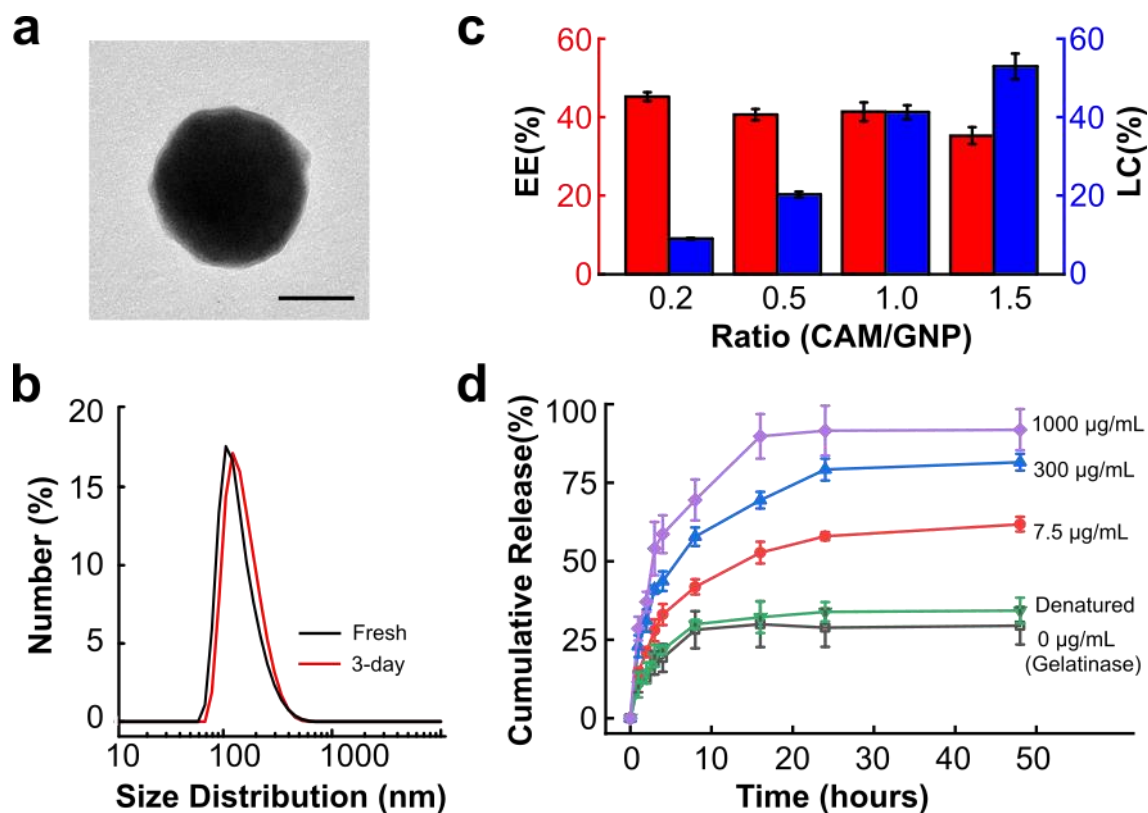


**Figure 2.** (a) TEM image of a gelatine nanoparticle (GNP). (b) Hydrodynamic size distribution of GNPs determined by dynamic light scattering. The black curve represents the freshly prepared sample and the red curve represents samples in storage for 3 days. (c) Drug loading capacity (LC) and encapsulation efficiency (EE) of GNPs with a weight ratio of chloramphenicol(CAM) to GNP of 0.2, 0.5, 1.0, and 1.5, respectively (d) Time-dependent CAM release curve of CAM@GNPs under different concentrations of gelatinase up to 48 hours. (scale bar: 50 nm).

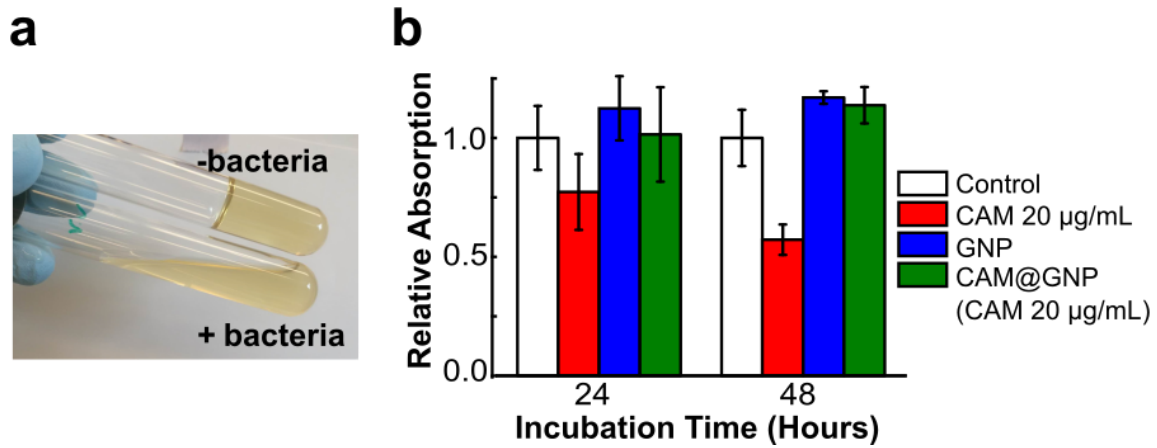


**Figure 3.** (a) Gelatine liquefaction test demonstrating the generation of gelatinase by bacteria (*V. vulnificus*). (b) Relative viable cell counts of NIH 3T3 fibroblasts after treatment with chloramphenicol solution (CAM), gelatin nanoparticles (GNPs), or CAM-encapsulated GNPs (CAM@GNPs), respectively (control as 1.0). (n=6).

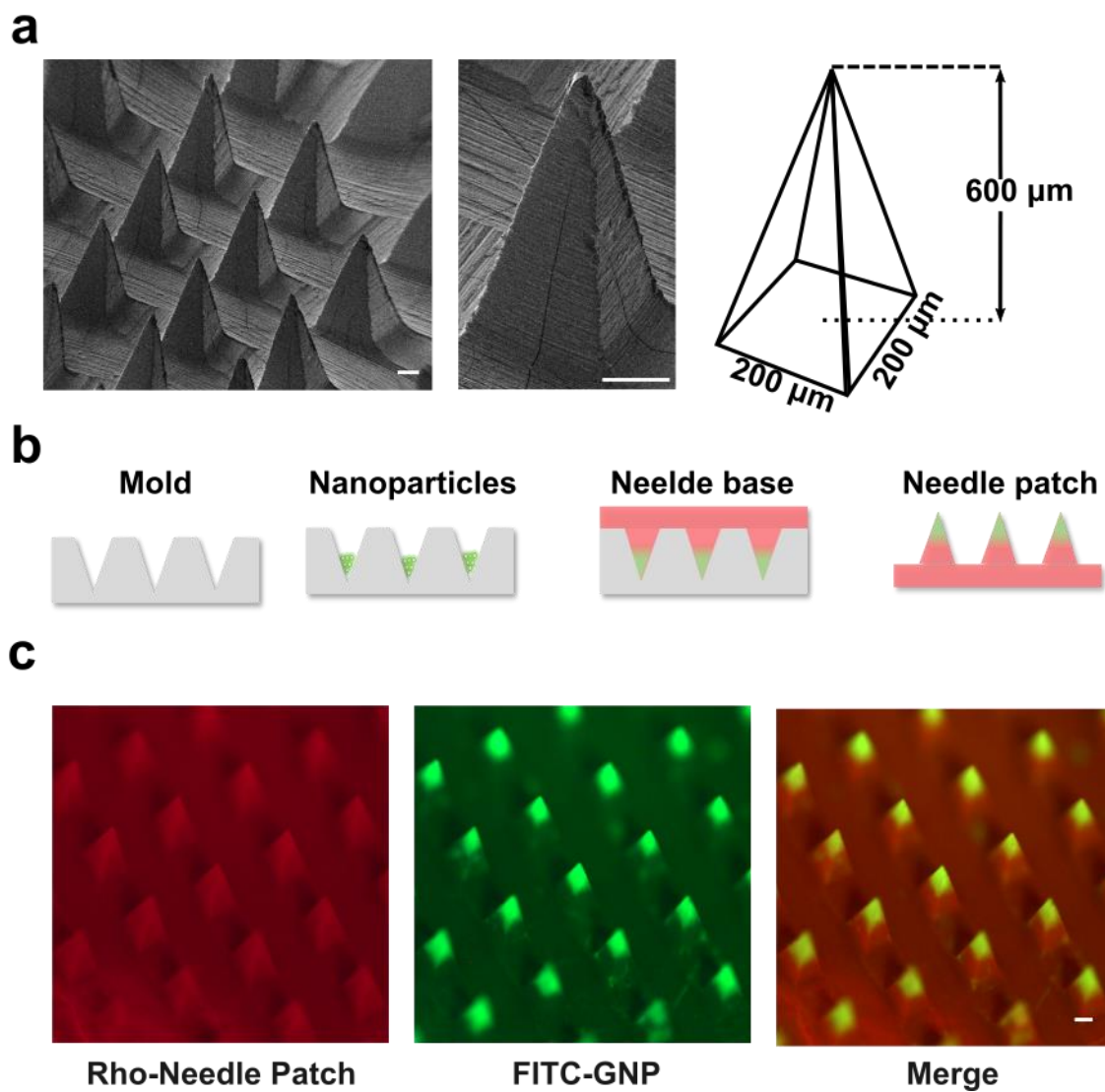


**Figure 4.** (a) SEM image of a microneedle patch. Right: Dimension of a single microneedle. (b) Schematic of nanoparticle-loaded microneedle patch fabrication process. (c) Fluorescence microscopy images of rhodamine B(Rho)-labeled microneedle patch loading FITC-labeled GNPs. Scale bar: 100  $\mu\text{m}$ .

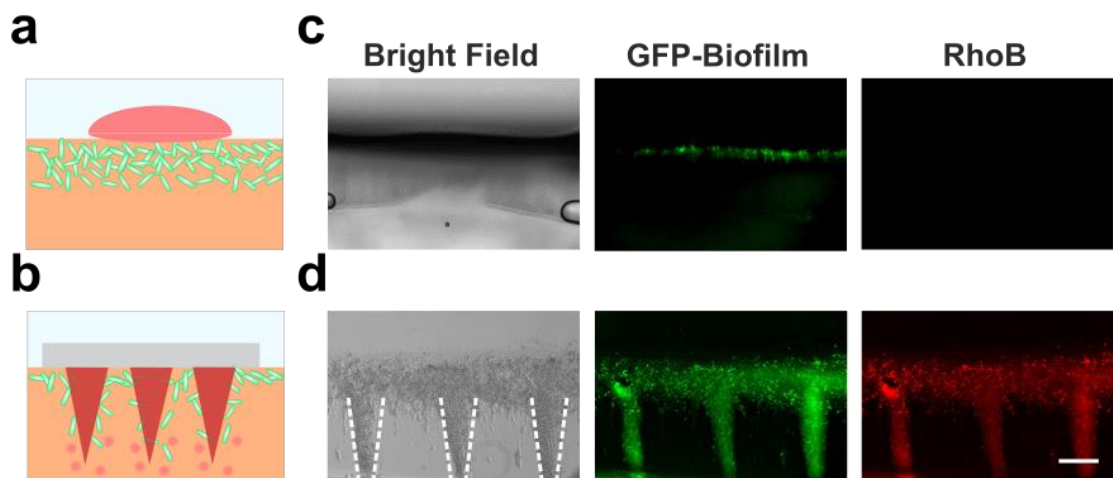


**Figure 5.** Schematics of (a) applying dye solution to biofilm or (b) microneedle patch inserting and releasing dye into biofilm. (c and d) Fluorescence microscopy images showing the spatial distribution of fluorescent molecules in GFP-labeled biofilm from (c) solution or from (d) the microneedle patch. The biofilm on penetration site was dissected and prepared on glass slides. Scale bar: 200  $\mu\text{m}$ .

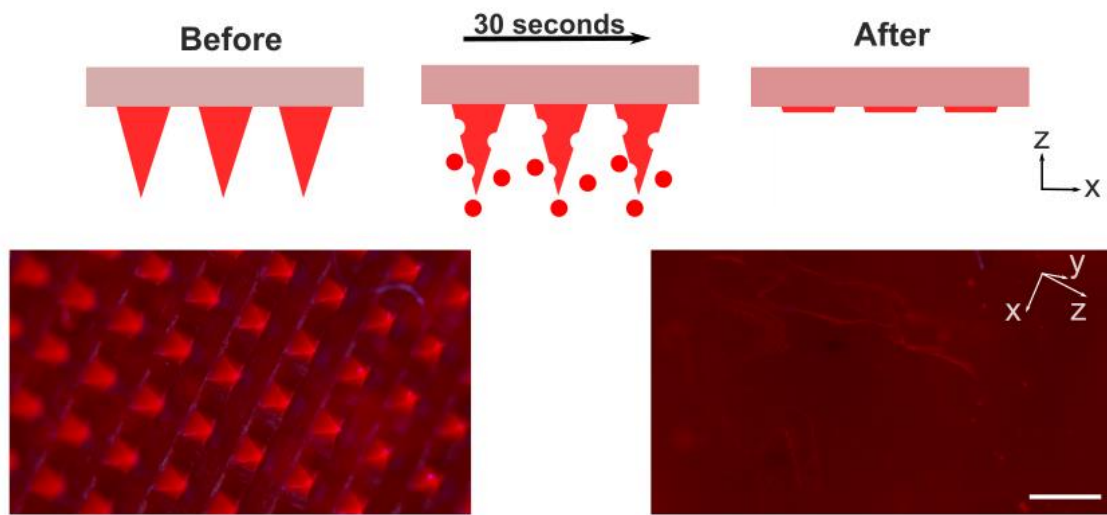


**Figure 6.** Microneedle patch inserting and releasing process. Bottom: optical images of microneedle patch before(left) and after(right) insertion into biofilm. Scale bar: 500  $\mu\text{m}$ .

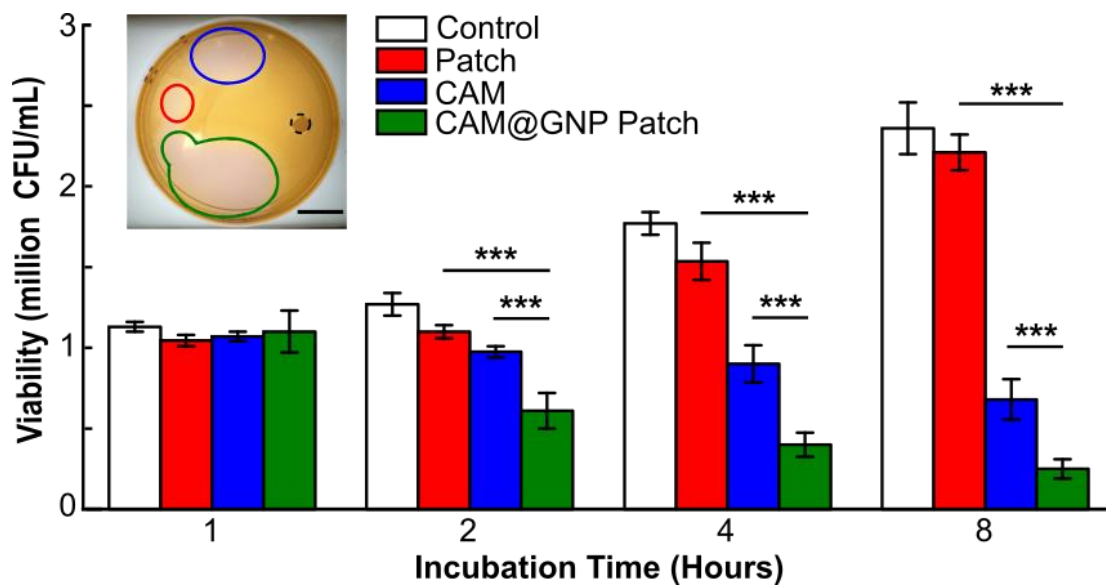


**Figure 7.** Viability of *V. vulnificus* biofilms after treatment with empty microneedle patch (Patch), CAM solution (CAM), and CAM@GNP-loaded microneedle patch (CAM@GNP Patch) for different treatment duration (CAM:20  $\mu$ g/mL). Insert: image of Petri dish showing zone of inhibition. \*\*\*P < 0.001 compared with the empty microneedle patch. Scale bar: 3 mm.